A COMPACT SCHEME FOR THE MUNK BOUNDARY-LAYER EQUATION IN ONE DIMENSION

M. BEN-ARTZI, J.-P. CROISILLE, AND D. FISHELOV

ABSTRACT. In this paper, we introduce a two-scale compact finite difference scheme for the equation

$$\text{(MK-1D)} \qquad \begin{cases} -\beta \dfrac{d}{dx} u + \varepsilon \Big(\dfrac{d}{dx} \Big)^4 u = f, \quad x \in (a,b) \\ u(a) = u(b) = u'(a) = u'(b) = 0. \end{cases}$$

This equation serves as a model for the nonlinear barotropic equation (NB) governing oceanic flows.

$$\text{(NB)} \qquad \partial_t \Delta \psi + \nabla^\perp \psi . \nabla \Delta \psi + \beta \partial_x \psi = \frac{1}{H} (\nabla \times \tau)_v - \mu \Delta \psi + \varepsilon \Delta^2 \psi,$$

where $\psi(x,y,t)$ and τ are the streamfunction and the wind stress tensor, respectively. This equation encodes the *western boundary layer problem* [13, 19] for the potential vorticity ψ, which corresponds to the sharp contrast between the gyres flow in the oceanic circulation at mid-latitude and the strong western boundary currents. Numerical results for Equation (MK-1D) show that, with this two-scale scheme, high order accuracy is preserved for u and $\Big(\frac{d}{dx} \Big) u$ both in the boundary layer and in the central zone of the domain. The test cases are taken from [8].

1. INTRODUCTION

The time dependent nonlinear barotropic dynamics equation is expressed as [17, Chap.3]

$$\partial_t \Delta \psi + \nabla^\perp \psi . \nabla \Delta \psi + \beta \partial_x \psi = \frac{1}{H} (\nabla \times \tau)_v - \mu \Delta \psi + \varepsilon \Delta^2 \psi. \tag{1.1}$$

The notation is as follows.

- $\psi(x,y,t)$ is the streamfunction and $\Delta \psi(t,x,y)$ is the vertical vorticity ($\Delta =$ 2D-Laplacian).
- $\nabla^\perp \psi = (-\partial_y \psi, \partial_x \psi) = (u,v)$ is the horizontal velocity. The convective term is $\nabla^\perp \psi . \nabla \Delta \psi = u \partial_x \Delta \psi + v \partial_y \Delta \psi$.
- $\varepsilon > 0$ is the lateral eddy viscosity. It encodes the shear wind friction effect at the surface of the ocean.
- $\mu \geq 0$ is a viscosity modelling the friction at ocean bottom.
- $\beta > 0$ is the constant of the Coriolis force. It depends on the latitude at which the so-called beta-plane hypothesis is applied.

Date: September 28, 2024.

2010 *Mathematics Subject Classification.* Primary 65L10; Secondary 65L70, 34K28.

Key words and phrases. Munk equation, boundary layer, compact scheme, Shishkin grid.

The authors thank the WSI for its support during the Thematic Program *The Dynamics of Planetary-Scale Flows* (Apr.11-Jun.02, 2023) and the organizers Profs. A. Constantin, D. Dritschel and N. Paldor.

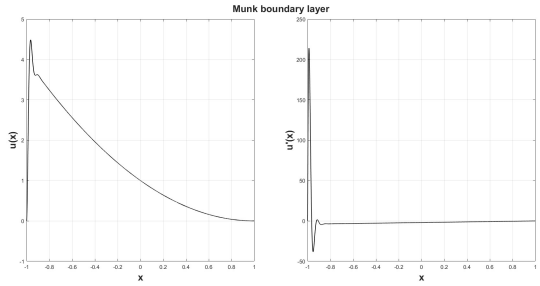

FIGURE 1. A typical profile of a solution $u(x)$ (left panel) and $\frac{d}{dx}u(x)$ (right panel) of a Munk boundary layer. The function $u(x)$ is (2.8) with parameter $p = 2$. The boundary conditions are $u(-1) = u(1) = u'(-1) = u'(1) = 0$.

- H is the depth of the ocean, assumed here to be constant.
- τ is the surface wind stress.

Equation (1.1) is a variant of the 2D Navier-Stokes equation in pure streamfunction formulation [4]. Assuming time independence, and that the convective term and bottom friction are negligible, leads to the two-dimensional linear problem posed e.g. in the rectangle $\Omega = (a, b) \times (c, d)$,

$$\text{(MK-2D)} \qquad \begin{cases} -\beta\partial_x\psi(x,y) + \varepsilon\Delta^2\psi(x,y) = f(x,y), \quad (x,y) \in \Omega \\ \psi = \partial_n\psi = 0, \quad (x,y) \in \partial\Omega. \end{cases}$$

Assuming independence in y, one obtains the one-dimensional version of the problem: find $x \in (a, b) \mapsto u(x)$, solution of

$$\text{(MK-1D)} \qquad \begin{cases} -\beta\dfrac{d}{dx}u + \varepsilon\Big(\dfrac{d}{dx}\Big)^4 u = f, \quad a < x < b, \quad (i) \\ u(a) = u(b) = u'(a) = u'(b) = 0, \quad (ii) \end{cases}$$

This is a biharmonic convection-diffusion problem, called the *Munk* equation with Dirichlet boundary conditions. The length parameter

$$\gamma = (\varepsilon/\beta)^{1/3} \tag{1.2}$$

relates the Coriolis force strenght to the eddy diffusion. The problem considered here is the design of an highly accurate compact finite difference scheme, able to approximate the two functions $u(x)$ and $\frac{d}{dx}u(x)$ depicted in Fig. 1, by solving (MK-1D) numerically. The scheme is designed so as to handle the limit $\gamma \to 0$. The smaller γ, the thinner the boundary layer. Usually in fluid mechanics, a boundary layer problem is associated to the convection diffusion equation, where the diffusion is the Laplacian operator. There is an important numerical analysis on this topic. We refer to the two mongraphs [9, 18]. In (MK-2D-MK-1D), the viscous term is biharmonic. This problem has received less attention. The recent [8] gives a nice account on on (MK-1D,MK-2D) from the theoretical and numerical viewpoints. See also [12]. Refer to [14] for a recent mathematical analysis account of boundary layers problems.

The outline of the paper is as follows. In Section 2, we give our reference scheme. Numerical results demonstrate that the error for u and u' are, as expected, fourth

order. However, as observed in [8], a prohibitive grid size is required to be "layer-resolving". Section 3 adresses this issue in the framework of compact schemes. A two-scale compact scheme is proposed on a Shishkin grid with two stepsizes. The coarse stepsize fits the "offshore" zone (the gyre zone, called the CZ zone hereafter). And the fine stepzise fits the thin boundary layer zone (called the BL zone). In Section 4, several numerical results using the test series in [8] show that high accuracy is retained both in the BL and CZ zones. Section 5 draws some perspectives.

2. A compact scheme for the Munk equation

2.1. **Design of the basic compact scheme.** Consider the Munk equation

$$\Big(\mathcal{L}u(x) \triangleq \Big) - \beta\frac{d}{dx}u(x) + \varepsilon\Big(\frac{d}{dx}\Big)^4 u(x) = f(x), \quad x \in \mathbf{R} \tag{2.1}$$

Denote $x_j = jh, j \in \mathbf{Z}$. A natural compact finite difference approximation for (2.1) is obtained as follows

(1) The derivative $\frac{d}{dx}u$ is approximated by the standard compact scheme

$$\frac{1}{6}\tilde{\delta}_x u_{j-1} + \frac{2}{3}\tilde{\delta}_x u_j + \frac{1}{6}\tilde{\delta}_x u_{j+1} = \delta_x u_j. \tag{2.2}$$

(2) The fourth order derivative $(\frac{d}{dx})^4 u$ is approximated by the Discrete Biharmonic Operator (DBO) δ_x^4 [1, 6]

$$\delta_x^4 u_j = \frac{12}{h^2}(\delta_x\tilde{\delta}_x u_j - \delta_x^2 u_j). \tag{2.3}$$

For the notation and properties of the operators $\tilde{\delta}_x$ and δ_x^4, refer to [1, 4, 6]. Using (2.2) and (2.3) yields the following approximation of (2.1) at node $j \in \mathbf{Z}$

$$\Big(\mathcal{L}_h u_j \triangleq \Big) - \beta\tilde{\delta}_x u_j + \varepsilon\delta_x^4 u_j = f_j, \quad j \in \mathbf{Z} \tag{2.4}$$

Since each operator $\tilde{\delta}_x$ and δ_x^4 has a 4th order truncation error, one expects a 4th order as well for the truncation error $\tau(u) = \Big(\mathcal{L}u\Big)^* - \mathcal{L}_h u^*$. One has [1]

$$\tau(u) = h^4\Big[\frac{\beta}{180}\Big((\frac{d}{dx})^5 u\Big)^* + \frac{\varepsilon}{720}\Big((\frac{d}{dx})^8 u\Big)^*\Big] + O(h^6). \tag{2.5}$$

Remark 2.1. *Here, one may wonder whether the original "single cell" approach of Stephenson* [20] *applied to (2.1), would lead to (2.4). This is actually the case, see Appendix 6.*

Consider now the problem (MK-1D) on the bounded interval $I = (0, 1)$. We use the standard notation with $N+1$ the total number of nodes, the stepsize $h = 1/N$, and the grid $x_j, j \in [\![0, N]\!]$. Our reference scheme consists of applying (2.4) at interior nodes $j = 2, \ldots, N-1$. A natural discrete couterpart of the 4 boundary conditions (MK-1D)(ii) is

$$u_0 = u_N = \tilde{\delta}_x u_0 = \tilde{\delta}_x u_N = 0. \tag{2.6}$$

[1] For u a given function, u^* denotes the gridfunction deduced from u by restriction to the grid.

With (2.6), there is no need of any ghost node or special treatment at the boundary. The final scheme is: solve in $[u_j], j \in [\![0, N]\!]$ the system

$$\begin{cases} -\beta\tilde{\delta}_x u_j + \varepsilon\delta_x^4 u_j = f_j, \;\; j = 1, \ldots, N-1, \\ \frac{1}{6}\tilde{\delta}_x u_{j-1} + \frac{2}{3}\tilde{\delta}_x u_j + \frac{1}{6}\tilde{\delta}_x u_{j+1} = \delta_x u_j \;\; j = 1, \ldots, N-1, \\ u_0 = u_N = \tilde{\delta}_x u_0 = \tilde{\delta}_x u_N = 0. \end{cases} \tag{2.7}$$

This scheme is the natural extension to (MK-1D) of the DBO scheme [4, chap. 10.3] Fourth order error estimate is expected [10]. Here however, we are interested in the specific regime $\beta \to \infty$ with $\varepsilon \to 0$, and such that $\gamma \to 0$. Oscillations are expected in the BL zone, and they indeed appear. This problem is observed in Section 2.2.

2.2. **Single grid numerical results.**

2.2.1. *The CHT Test Case for the Munk equation.* We consider the set of solutions (called CHT functions) (2.8) suggested in [8] defined by

$$u(x) = \Big(1 - \frac{1}{\sqrt{3}}Q_1(x,\gamma) - Q_2(x,\gamma)\Big)(1-x)^2, \quad x \in (-1,1), \tag{2.8}$$

with

$$\begin{cases} Q_1(x,\gamma) = \exp\Big(-\frac{x+1}{2\gamma}\Big)\sin\Big(-\frac{\sqrt{3}(x+1)}{2\gamma}\Big), \\ Q_2(x,\gamma) = \exp\Big(-\frac{x+1}{2\gamma}\Big)\cos\Big(-\frac{\sqrt{3}(x+1)}{2\gamma}\Big). \end{cases} \tag{2.9}$$

The velocity β, viscosity ε and length γ are given by the sequence

$$(\beta_p, \varepsilon_p, \gamma_p) = (10^{2p}, 10^{-p}, 10^{-p}), \;\; p \geq 0. \tag{2.10}$$

The function (2.8) provides a set of test cases with parameter p. The larger p, the smaller γ, the thinner the boundary layer and the more difficult the test. The forcing function f in (MK-1D) is obtained by (hand manufacturing method)

$$f(x) \triangleq \mathcal{L}u(x). \tag{2.11}$$

Refer to [8] for the expression of $f(x)$. Select first $p = 1$ in (2.10). This corresponds to $(\beta, \varepsilon, \gamma) = (100, 0.1, 0.1)$. In this case, Equation (MK-1D) is a regular 4th order ODE. Table 1 exhibits an expected 4th order convergence rate as well as accurate error levels for u and $\frac{d}{dx}u$ using the coarse grid sequence $N = 20, 40, 80, 160$. The notation for the relative errors $\mathfrak{e}, \mathfrak{e}_x$ and for the maximum grid norm is

(2.12)
$$\begin{cases} \mathfrak{e}_j = |u^*(x_j) - \mathfrak{u}_j| / \max\limits_{-1<x<1} |u(x)|, \;\; \mathfrak{e}_{x,j} = \Big|\Big(\frac{d}{dx}u\Big)^*(x_j) - \tilde{\delta}_x \mathfrak{u}_j\Big| / \max\limits_{-1<x<1} |u'(x)|, \\ |\mathfrak{v}|_\infty = \max\limits_{1\leq j\leq N-1} |\mathfrak{v}_j|. \end{cases}$$

The cases $p = 2$ and $p = 3$ serve to illustrate the numerical difficulty with the scheme (2.7) for the Munk problem (MK-1D).

mesh	20	Rate	40	Rate	80	Rate	160
$\lvert\mathfrak{e}\rvert_\infty$	4.3529(-3)	3.85	3.0202(-4)	3.99	1.9060(-5)	4.00	1.1940(-6)
$\lvert\mathfrak{e}_x\rvert_\infty$	7.4202(-3)	4.23	3.9564(-4)	4.06	2.3706(-5)	4.02	1.4659(-6)

TABLE 1. Test case (2.8) with $p = 1$ for the Munk equation (MK-1D). Relative maximum errors $|\mathfrak{e}|_\infty$ and $|\mathfrak{e}_x|_\infty$ are reported, when using (2.7). A standard 4th order accuracy is observed with good error levels.

2.2.2. *Case* $p = 2$. This case corresponds to $(\beta, \varepsilon, \gamma) = (10^4, 10^{-2}, 10^{-2})$. Consider first the grid sequence $N = 20, 40, 80, 160$. This sequence is too coarse to approximate the BL zone, even qualitatively. Fig. 2 top shows the relative errors for u and $\frac{d}{dx}u$. Typical numerical oscillations are displayed with two subsequences observed. Note however that even with only two nodes in the boundary layer, the numerical derivative $\tilde{\delta}_x u$ displays a somehow acceptable behaviour, considering the magnitude of the function. With a grid size $N = 160$ (Fig. 2 bottom) the profiles of u and $\frac{d}{dx}u$ are accurately reproduced, with only 6 nodes in the BL zone. Fig. 3 exhibits convergence slopes for the unresolved grid sequence $N = 20, 40, 80, 160$ (top) and for the resolved grid sequence $N = 160, 320, 640, 1280$ (bottom). An expected order 4 for u and $\frac{d}{dx}u$ is observed And on the top, it is observed that some grid convergence slope can coexist with a nonconverged behaviour for u.

2.2.3. *Case* $p = 3$. This case corresponds to $(\beta, \varepsilon, \gamma) = (10^6, 10^{-3}, 10^{-3})$. With $N = 400$, the scheme is layer-unresolved and oscillations similar to Fig. 3 top do appear, (not shown). The grid $N = 800$ displays a resolved BL zone. And Fig. 4 top shows the convergence slopes for the unresolved grid sequence $N = 100, 200, 400, 800$. Fig. 3 bottom shows the case of the layer-resolved grid sequence $N = 800, 1600, 3200, 6400$.

2.3. **Comments.** Here are some observations drawn from the numerical results in Section 2.2.

(1) It is well known that discretizing $\mathcal{L} \triangleq \beta\partial_x - \varepsilon\partial_x^2$ by the centered operator $\mathcal{L}_h \triangleq \beta\delta_x - \varepsilon\delta_x^2$, leads to oscillations in the numerical boundary layer, see e.g. [15, Chap.3]. Here oscillations do appear when the value h/γ (the Peclet number in the present context) is large.
(2) For fixed values of ε and β a 4th order asymptotic convergence rate takes place when $h \to 0$. This is of little help in practice. In the case $p = 3$ a typical layer-resolved grid must be of size $N \simeq 4000$, as observed in Fig. 4. However, a grid of $N = 4000$ results in a matrix corresponding to (2.7), of size 8000×8000 (two unknowns per node), which is prohibitive for a 1D problem.
(3) A convergent slope can coexist with oscillations. Therefore, a convergent slope, possibly high order, is no guaranty that the results are accurate with the finest grid. In that case, attention must be paid to the error level.

3. A two-scale compact scheme for the Munk equation

3.1. **Two-domain compact scheme approach.** We present an extension of the compact scheme (2.7) based on the splitting of the interval $I = (a, b)$ into two parts,

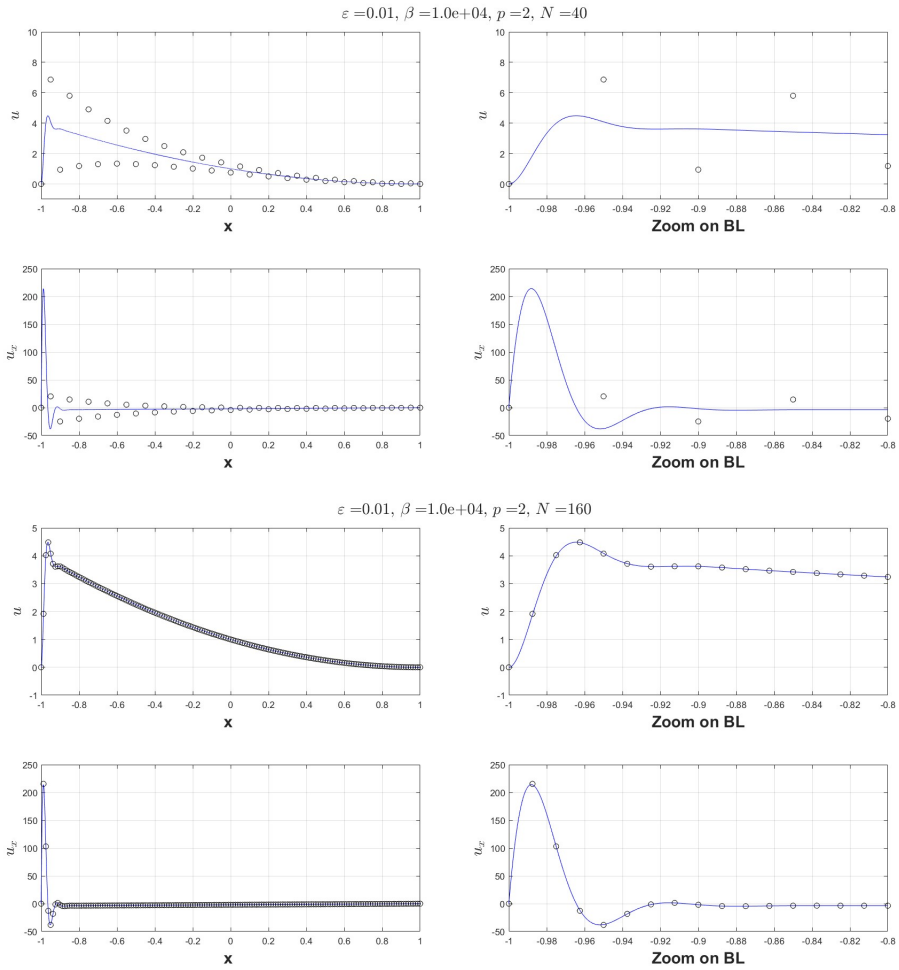

FIGURE 2. Test case (2.8) with $p = 2$ for the Munk equation (MK-1D). Top: behaviour of the scheme for u and $\frac{d}{dx}u$ with the underresolved grid $N = 40$: the underresolution is characterized by two subsequences visible on the approximations of u and $\frac{d}{dx}u$. Bottom: behaviour of the scheme for u and $\frac{d}{dx}u$ with the grid $N = 160$. The results are visually satisfactory.

see Fig. 5. Two contiguous grids are used, denoted as

$$\begin{cases} x_0^{\mathrm{BL}} \triangleq a, x_1^{\mathrm{BL}} \triangleq a+h, \ldots, x_{N-1}^{\mathrm{BL}} \triangleq c-h, \ldots, x_N^{\mathrm{BL}} \triangleq c \\ \bar{x}_0^{\mathrm{CZ}} \triangleq c, \bar{x}_1^{\mathrm{CZ}} \triangleq c+\bar{h}, \ldots, x_{\bar{N}-1}^{\mathrm{CZ}} \triangleq b-\bar{h}, \ldots, x_{\bar{N}}^{\mathrm{CZ}} \triangleq b. \end{cases} \tag{3.1}$$

The interconnecting node $x_N^{\mathrm{BL}} = x_{\bar{0}}^{\mathrm{CZ}} = c$ is called the *transmission* node. The basic scheme (2.7) is used in zones BL and CZ with stepsize h and $\bar{h}$, respectively. In what follows, we define a specific scheme at the transmission node c. This kind of two-scale grid belongs to the so-called Shishkin grids, (piecewise constant stepsize). See [9] and the references therein. Hereafter, we explore a scheme design based on

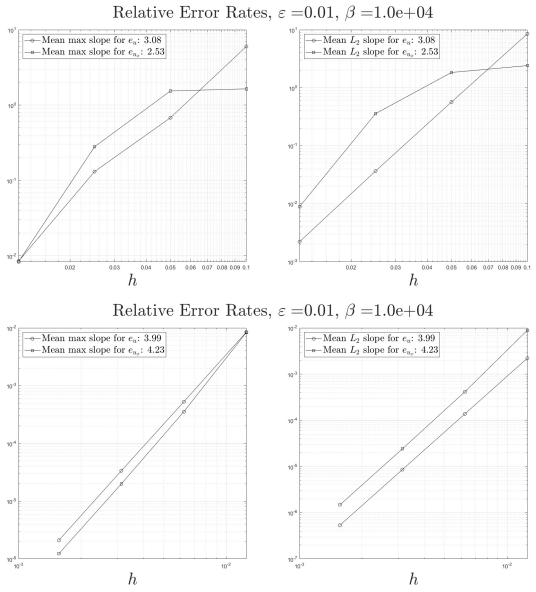

FIGURE 3. Test case (2.8) with $p = 2$ for the Munk equation (MK-1D). Top panel: convergence rate for e and e_x with the grid sequence $N = 20, 40, 80, 160$. This grid sequence corresponds to an underresolved BL. However, underresolution can coexist with some grid convergent slope. Bottom panel: convergence rate for e and e_x with the grid sequence $N = 160, 320, 640, 1280$. This grid sequence corresponds to a resolved boundary layer. 4th order convergence for e and e_x is observed as well as error levels less than 10^{-6} for u and $\frac{d}{dx}u$.

a particular set of high order polynomials. Our guideline consists of the observed numerical errors obtained for (2.8) with low values of γ. In Section 3.2 we present the transmission scheme giving the most accurate results so far.

3.2. **A two-scale extension of the Discrete Biharmonic Operator.** In Sections 3.2.1 and 3.2.2 interpolatory polynomials called $q(x)$ and $r(x)$ are introduced. They serve to define the operators $\hat{\delta}_x$ and $\hat{\delta}_x^4$, respectively, in the spirit of compact schemes. These operators are used at the transmission node c in (3.15) hereafter.

3.2.1. *The polynomial $q \in \mathcal{P}_4$.* Here and in Section 3.2.2, we call x_j a general grid with non equispaced stepsize. At each node is attached a couple of values $(u_j, u_{x,j})$ approximating $u(x_j)$ and and $\frac{d}{dx}u(x_j)$, where u is a given function. Define as in [3] the polynomial $q \in \mathcal{P}_4$

$$q(x) = b_0 + b_1(x - x_j) + b_2(x - x_j)^2 + b_3(x - x_j)^3 + b_4(x - x_j)^4, \tag{3.2}$$

fitting the 5 data near x_j

$$\begin{cases} q(x_{j-1}) = u_{j-1}, \;\; q(x_j) = u_j, \quad q(x_{j+1}) = u_{j+1}, \\ q'(x_{j-1}) = u_{x,j-1}, \;\; q'(x_{j+1}) = u_{x,j+1}. \end{cases} \tag{3.3}$$

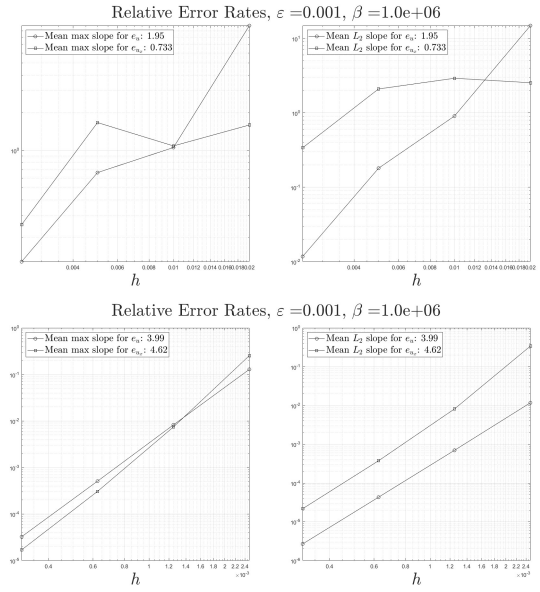

FIGURE 4. Test case (2.8) with $p = 3$ for the Munk equation (MK-1D). Top panel: convergence rate for e and e_x with the grid sequence $N = 100, 200, 400, 800$. Underresolution can coexist with some convergence. Bottom panel: convergence rate for e and e_x with the grid sequence $N = 800, 1600, 3200, 6400$. This grid sequence corresponds to a resolved boundary layer. A 4th order convergence for e and e_x is observed

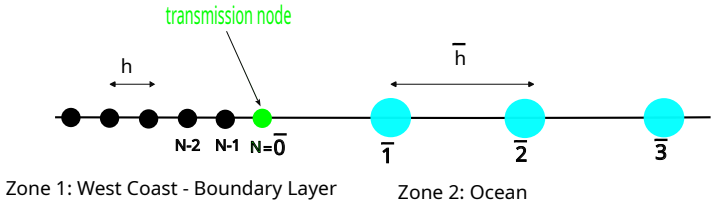

FIGURE 5. Shishkin two-scale Finite Difference grid. Fine grid: $0 \le j \le N$; Coarse grid: $0 \le \bar{j} \le \bar{N}$. The transmission node is at $x_N = x_{\bar{0}} = c$.

With the definition $h_1 \triangleq x_j - x_{j-1}$ and $h_2 \triangleq x_{j+1} - x_j$ and

$$\begin{cases} \alpha_{1,j} = \dfrac{h_2^2}{(h_2+h_1)^2}, \quad \alpha_{2,j} = \dfrac{h_1^2}{(h_2+h_1)^2}, \quad \beta_{2,j} = \dfrac{2(h_2-h_1)}{h_1 h_2}, \\ \beta_{1,j} = -\dfrac{2h_2^2(2h_1+h_2)}{h_1(h_1+h_2)^3}, \quad \beta_{3,j} = \dfrac{2h_1^2(2h_2+h_1)}{h_2(h_1+h_2)^3}. \end{cases} \tag{3.4}$$

we obtain that the coefficient $b_1 = q'(x_j)$ in (3.2) is expressed as

$$b_1 = \beta_{1,j}u_{j-1} + \beta_{2,j}u_j + \beta_{3,j}u_{j+1} - (\alpha_{1,j}u_{x,j-1} + \alpha_{2,j}u_{x,j+1}). \tag{3.5}$$

Defining $\hat{\delta}_x u_j \triangleq b_1$ extends to the irregular case the standard formula (2.2). It was proved in [3] that it is 4th order accurate with respect to $\frac{d}{dx}u(x_j)$, assuming uniform lower and upper bounds on h_1/h_2.

3.2.2. *The polynomial $r \in \mathcal{P}_7$ for $\hat{\delta}_x^4$.* Similarly to Section 3.2.1, we define a Discrete Biharmonic Operator (DBO) approximating $(\frac{d}{dx})^4(x_j)$ at

$$x_j \triangleq c = x_N^{\mathrm{BL}} = \bar{x}_{\bar{0}}^{\mathrm{CZ}}, \tag{3.6}$$

based on data on the irregular grid shown in Fig. 5. On a regular grid, the standard DBO δ_x^4 satisfies at an internal node, called $j-1$, the relation [4, Sect. 10.4]

$$\sigma_x \delta_x^4 u_{j-1} = (\delta_x^2)^2 u_{j-1}. \tag{3.7}$$

The relation (3.7) is expressed as

$$\frac{1}{6}\delta_x^4 u_{j-2} + \frac{2}{3}\delta_x^4 u_{j-1} + \frac{1}{6}\delta_x^4 u_j = \frac{1}{h^4}(u_{j+1} - 4u_j + 6u_{j-1} - 4u_{j-2} + u_{j-3}). \tag{3.8}$$

This yields at node j the identity

$$\delta_x^4 u_j = \frac{6}{h^4}(u_{j+1} - 4u_j + 6u_{j-1} - 4u_{j-2} + u_{j-3}) - \delta_x^4 u_{j-2} - 4\delta_x^4 u_{j-1}. \tag{3.9}$$

Consider the regular grid on the BL zone (left of x_j). And consider the Lagrange polynomial $r(x) \in \mathcal{P}_7$

(3.10)
$$r(x) = a_0 + a_1 + a_2(x-x_j)^2 + a_3(x-x_j)^3 + a_4(x-x_j)^4 + a_5(x-x_j)^5 + a_6(x-x_j)^6 + a_7(x-x_j)^7$$

fitting the 8 data

(3.11)
$$\begin{cases} r(x_j) = u_j, \;\; r(x_{j-1}) = u_{j-1}, \;\; r(x_{j-2}) = u_{j-2}, \;\; r(x_{j-3}) = u_{j-3}, \;\; r(x_{j-4}) = u_{j-4}, \\ r(x_{j+1}) = u_{j+1}, \;\; r(x_{j+2}) = u_{j+2}, \;\; r(x_{j+3}) = u_{j+3}. \end{cases}$$

We have denoted $x_{j+ph} = c + ph$, $p \in [\![-4:3]\!]$. In order to use (3.9) to define a suitable DBO at x_j, we need some approximation $\tilde{u}_{j+1}$ at $x_j + h$ in terms of data belonging to the two grids in Fig. 5. This is obtained by

$$\tilde{u}_{j+1} \triangleq r_{u_{j+p}, p\in[\![-4:3]\!]}(x_j + h). \tag{3.12}$$

Invoking $\tilde{u}_{j+1}$ defined in this way, the extended DBO is defined by

$$\widehat{\delta}_x^4 u_j \triangleq \frac{6}{h^4}(\tilde{u}_{j+1} - 4u_j + 6u_{j-1} - 4u_{j-2} + u_{j-3}) - \delta_x^4 u_{j-2} - 4\delta_x^4 u_{j-1}. \tag{3.13}$$

A 4th order truncation (in the periodic setting) of the extended DBO is expressed in terms of h and R by

$$\widehat{\delta}_x^4 u_j - \Big((\frac{d}{dx})^4 u\Big)_j^* = \frac{1}{5040}(540R^3 - 990R^2 + 540R - 97)\Big((\frac{d}{dx})^8 u\Big)_j^* h^4 + O(h^5), \tag{3.14}$$

The truncation of the standard DBO (2.3) in recovered in the particular case $R = 1$.

3.3. **Two-scale compact scheme for the Munk equation.** Consider again the equation (MK-1D). Let $c \in (a,b)$ be fixed. Recall that a fine grid with N intervals covers the BL zone (a,c) with stepsize $h=(c-a)/N$ and a coarse grid is layed out on $(c,1)$ with $\bar{N}$ intervals. Assume $h<\bar{h}$ with $R=\bar{h}/h>1$. The full grid contains $N+\bar{N}$ intervals in all on $(a,b)=(-1,1)$. The equation (MK-1D) is approximated with the scheme

$$
\begin{cases}
-\beta\tilde{\delta}_x u_j+\varepsilon\delta_x^4 u_j=f_j^*, \;\; 1\le j\le N-1, \;\; x_j\in(a,c), \;\; \text{BL zone}\\
-\beta\widehat{\delta}_x u_N+\varepsilon\widehat{\delta}_x^4 u_N=f_N^*, \;\; x_N=c= \text{ transmission node}\\
-\beta\tilde{\delta}_x u_j+\varepsilon\delta_x^4 u_j=f_j^*, \;\; N+1\le j\le N+\bar{N}-1, \;\; \text{CZ zone}\\
u_0=u_{N+\bar{N}}=\tilde{\delta}_x u_0=\tilde{\delta}_x u_{N+\bar{N}}=0.
\end{cases}
\tag{3.15}
$$

The scheme (3.15) is obtained by using (2.7) with the operators $\tilde{\delta}_x$ and δ_x^4 at the $N-1$ nodes in $x_j\in(a,c)$ with step size h. And similarly at the $\bar{N}-1$ nodes $x_j\in(c,b)$ with stepsize $\bar{h}$. The hybrid scheme using the operators $\hat{\delta}_x$ and $\hat{\delta}_x^4$ is used only at the transmission node $x_N=c$. The linear system to be solved consists of the $N+\bar{N}-1$ equations (3.15) and of the $N+\bar{N}-1$ equations relating the Hermitian derivative $\tilde{\delta}u_{x,j}$ to the values u_j. This is another $N+\bar{N}-1$ equations. Adding the 4 boundary conditions, yields a linear system of size $(2N+2\bar{N})\times(2N+2\bar{N})$.

4. Numerical results

In this section, we show numerical results for the scheme (3.15) to approximate (MK-1D) on the interval $(a,b)=(-1,1)$. The test (2.8) with the values $p=3,4,5$. For these three values, the single grid scheme (2.7) is not practical since the required number of nodes to obtain accuracy is prohibitive. In each case, the test has been performed with several empirical principles. First, the transmission node $c=x_N$ is located sufficiently far from the BL zone. A factor of at least 10 times the width of the BL zone has been found appropriate. Second, computer accuracy has been reached as much as possible in the CZ zone. This has been found a good indicator that the results are accurate as well in the BL zone. Figs. 6 7 and 8 display the results for $p=3$, $p=4$ and $p=5$, respectively. In each case and for each grid sequence, we have:

- The shape in the transition zone as well as a zoom in the BL zone for $u(x)$ and $\frac{d}{dx}u$ is shown, for a coarse and a fine grid. The coarse to fine ratio $R=\bar{h}/h$ is given as well as the location of the transmission node c.
- The convergence rate of the relative error in the zones BL and CZ are given for u and $\frac{d}{dx}u$ for the maximum norm is shown. The l^2 norm has a similar shape and is not shown.
- The values $p=4$ and $p=5$ correspond to a very sharp behaviour in the BL zone. This is the most difficult cases [8]. The coarsest grid almost solves the CZ zone at computer accuracy. It is observed that this induces 4th order convergence in the BL zone.

5. Conclusion

In this paper, a compact scheme for the Munk equation with a thin boundary layer has been introduced. Our goal is to investigate how to preserve the high accuracy of the compact DBO in a two-scale Cartesian grid setting. Numerical results

obtained so far seem promising. Our scheme is an alternative to the "enriched" approach in [8], where an analytical knowledge of the layer is introduced in the approximation. In terms of finite differencing, our focus has been to investigate which strategies give the better accuracy for the solution u and the derivative $\frac{d}{dx}u$. Regarding boundary layer approximations, the experimental point of view is considered as important in [9], as well for the scheme design as for the convergence analysis. Future work includes continuing our experimental analysis for (MK-1D), (MK-2D) and for nonlinear variants, on multiscale grids. On the other hand, the numerical analysis seems a difficult question. In this regard, analytical tools in [5, 7, 9, 11, 16, 18] will be obviously useful.

6. Appendix: Stephenson approach for a compact scheme for the Munk problem.

Here we look back to the original methodology of Stephenson [20] originally introduced to design discrete biharmonic operators on Cartesian grids. The *single cell* associated to the node x_j is the compact interval $I_j = [x_{j-1}, x_{j+1}]$. Let $p(x) \triangleq a_0 + a_1(x-x_j) + a_2(x-x_j)^2 + a_3(x-x_j)^3 + a_4(x-x_j)^4$, as the so-called *embedding polynomial* associated to x_j, defined on I_j. The design proceeds as follows. First, assume that the *global unknowns* are the values called u_j and $u_{x,j}$, located at node j. If $u(x)$ is the continuous function to be approximated, one has $u(x_j) \simeq u_j$ and $(\frac{d}{dx}u)(x_j) \simeq u_{x,j}$. In our context, the polynomial p plays the role of a local model for (MK-1D) within the cell I_j. The 5 identities are imposed:

$$\begin{cases} p(x_{j+1}) = u_{j+1}, \;\; p(x_{j-1}) = u_{j-1}, & (a) \\ p'(x_{j+1}) = u_{x,j+1}, \;\; p'(x_{j-1}) = u_{x,j-1}, & (b) \\ -\beta p'(x_j) + \varepsilon p^{(4)}(x_j) = f(x_j), & (c) \end{cases} \tag{6.1}$$

Equations (a) and (b) are discrete boundary conditions on I_j. The relation (c) plays the role of the discrete Munk equation at x_j. In the standard derivation of a compact schemes [4], the identity $p(x_j) = u_j$ in used in place of (c). It leads to independent discrete operators instead of the "equation dependent" scheme (6.1). The coefficients $[a_k]_{0\le k\le 4}$ satisfy the relations:

(6.2)
$$\begin{cases} a_0 + a_1 h + a_2 h^2 + a_3 h^3 + a_4 h^4 = u_{j+1}, \;\; a_0 - a_1 h + a_2 h^2 - a_3 h^3 + a_4 h^4 = u_{j-1}, \\ a_1 h + 2a_2 h + 3a_3 h^2 + 4a_4 h^3 = u_{x,j+1}, \;\; a_1 h - 2a_2 h + 3a_3 h^2 - 4a_4 h^3 = u_{x,j-1}, \\ -\beta a_1 + 24\varepsilon a_4 = f(x_j). \end{cases}$$

The coefficients a_0, a_1 are related to the global data by

$$a_0 = p(x_j) = u_j, \quad a_1 = p'(x_j) = u_{x,j}. \tag{6.3}$$

Solving (6.2) yields the two relations

$$\begin{cases} a_1 = \dfrac{3}{4h}(u_{j+1} - u_{j-1}) - \dfrac{1}{4}(u_{x,j+1} + u_{x,j-1}) \\ u_j = \dfrac{1}{2}\Big[\dfrac{h^4}{12}\dfrac{1}{\varepsilon}(f_j + \beta u_{x,j}) - \dfrac{1}{2}(u_{x,j+1} - u_{x,j-1}) + u_{j+1} + u_{j-1}\Big]. \end{cases} \tag{6.4}$$

It turns out that the relations (6.4) are equivalent to the scheme (2.2)-(2.4) at node x_j.

References

[1] M. Ben-Artzi, J-P. Croisille and D. Fishelov, Convergence of a compact scheme for the pure streamfunction formulation of the unsteady Navier-Stokes system, SIAM J. Num. Anal., 44, 5, 1997–2024, (2006).

[2] M. Ben-Artzi, J-P. Croisille and D. Fishelov, A Cartesian compact scheme for the Navier-Stokes equations in streamfunction formulation in irregular domains, J. Sci. Comp. **81(3)** (2019), 1386–1408.

[3] M. Ben-Artzi, I. Chorev, J-P. Croisille and D. Fishelov, A compact difference scheme for the biharmonic equation in planar irregular domains", SIAM J. Num. Anal., **47**, (2009), 3087–3108.

[4] M. Ben-Artzi, J.-P. Croisille and D. Fishelov, "Navier-Stokes Equations in Planar Domains", Imp. Coll. Press, 2013.

[5] M. Ben-Artzi, J-P. Croisille, D. Fishelov and R. Katzir, Discrete fourth-order Sturm-Liouville problems, IMA J. Num. Anal. **38** (2018), 1485–1522. doi: 10.1093/imanum/drx038

[6] M. Ben-Artzi and G. Katriel, Spline functions, the biharmonic operator and approximate eigenvalues, Num. Math., **141** (2019), 839–879.

[7] M. Ben-Artzi and B. Kramer, Finite difference approach to fourth-order linear boundary value problems, IMA J. Num. Anal. **41** (2021), 2530–2561. doi: 10.1093/imanum/draa057

[8] M.D. Chekroun, Y. Hong and R.M. Temam, Enriched numerical scheme for singularly perturbed quasi-geostrophic equations, J. Comp. Phys. **416** (2020), 109493.

[9] P.A. Farrell, A.E. Hegarty, J.J.H. Miller, E. O'Riordan, G.I. Shishkin: *Robust computational techniques for boundary layers* (1st ed). Chapman and Hall CRC, 2000

[10] D. Fishelov, M. Ben-Artzi and J-P. Croisille, Recent advances in the study of a fourth-order compact scheme for the one-dimensional biharmonic equation, J. Sci. Comp. **53** (2012), 55–79.

[11] D. Fishelov and J-P. Croisille, Optimal convergence for time dependent Stokes equation: A new approach, J. Sci. Comp. **89** (2021), https://doi.org/10.1007/s10915-021-01684-955–79.

[12] S. Franz and H-G. Roos, Robust error estimation in energy and balanced norms for singularly perturbed fourth order problems, Comp. Math. App., **72** (2016), 233-247.

[13] M. Ghil, M. D. Chekroun and E. Simonnet , Climate dynamics and fluid mechanics: natural variability and related uncertainties, Physica D **237** (2008), 2011–2126.

[14] G-M. Gie, M. Hamouda, C-Y Jung and R. M. Temam, Singular Perturbations and Boundary Layers, AMS 200, Springer, 2018.

[15] C. Johnson, Numerical solutions of partial differental equations by the finite element method, Cambridge Univ. Press, 1987.

[16] B.S. Jovanović and E. Suli, "Analysis of Finite Difference Schemes for Linear Partial Differential Equations", Springer, 2014.

[17] J. McWilliams , Oceanic Circulation, AOS25 Courses Notes, 2006.

[18] H-G. Roos, M. Stynes, L. Tobiska, *Robust Numerical Methods for Singularly Perturbed Differential Equations* , Springer-Verlag, Berlin, 2008.

[19] E. Simonnet, M. Ghil and H. Dijkstra, Homoclinic bifurcations in the quasi-geostrophic double-gyre circulation, J. Mar. Res. **63** (2005), 931–956.

[20] J.W. Stephenson, Single cell discretizations of order two and four for biharmonic problems, J. Comput. Phys., 55, 1984, 65–80

Matania Ben-Artzi: Institute of Mathematics, The Hebrew University, Jerusalem 91904, Israel

Email address: mbartzi@math.huji.ac.il

Jean-Pierre Croisille: 1. Univ. Lorraine, IECL, UMR 7502, Metz F-57045, France - 2. CNRS, IECL, UMR 7502, Metz, F-57045, France

Email address: jean-pierre.croisille@univ-lorraine.fr

Dalia Fishelov: Afeka College of Engineering, 218 Bnei-Efraim St., Tel Aviv 69107, Israel

Email address: daliaf@afeka.ac.il

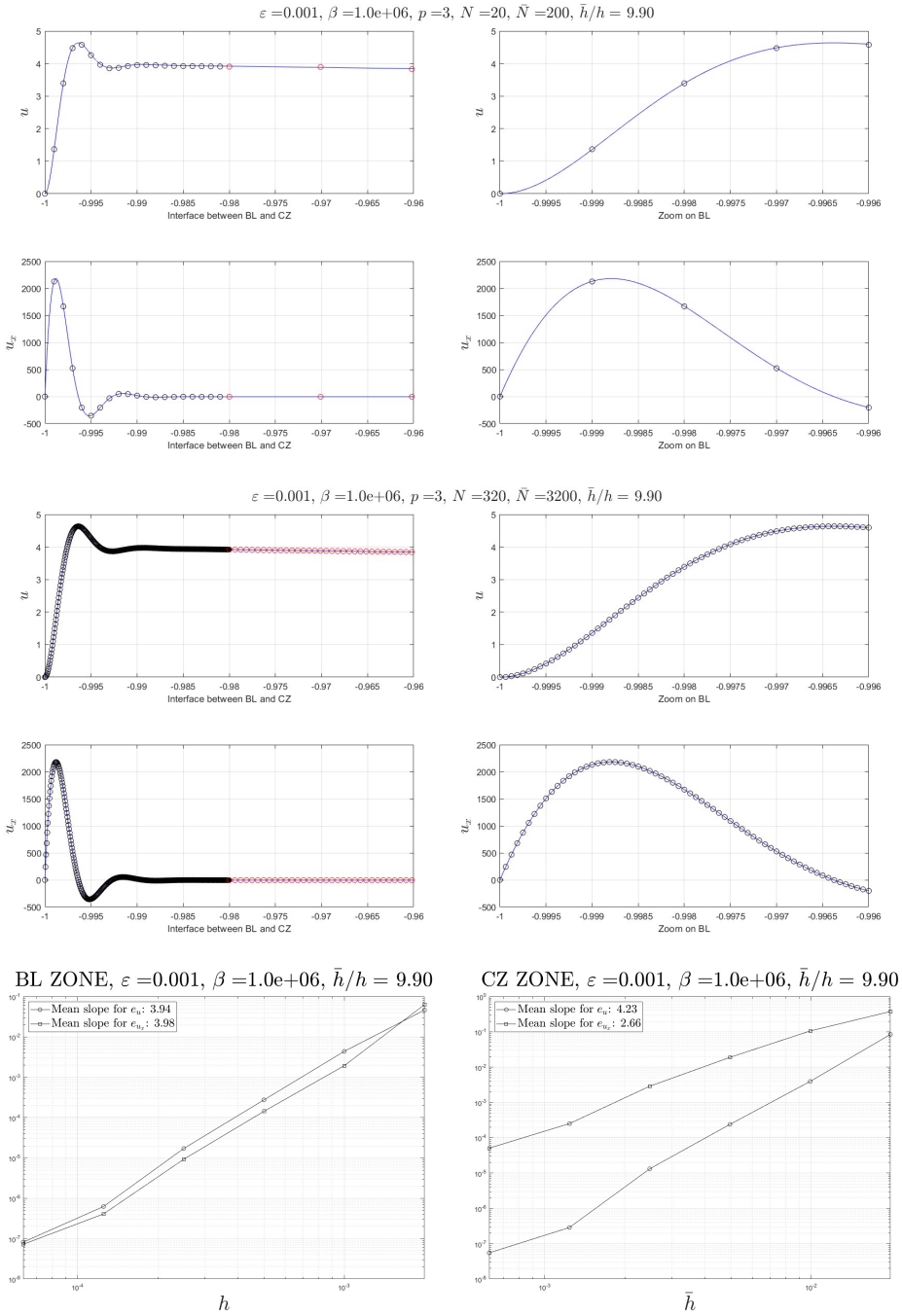

FIGURE 6. Munk-Stommel Equation (MK-1D) discretized with the scheme (3.15). Test case (2.8) with $p = 3$, $\varepsilon = 10^{-3}$, $\beta = 10^6$, $\gamma = 10^{-3}$. Coarse to fine grid ratio $\bar{h}/h = R = 10$. Convergence is analyzed with grid sequence $(N, \bar{N})$ is $(10, 100), (20, 200), (40, 400), (80, 800), (160, 1600), (320, 3200)$. The transmission node is located at $c = -0.98$. The convergence rate is around 4 in BL and the CZ zones. The maximum relative error is close to 10^{-7} for u and u' in the BL and CZ zones with the finest grid.

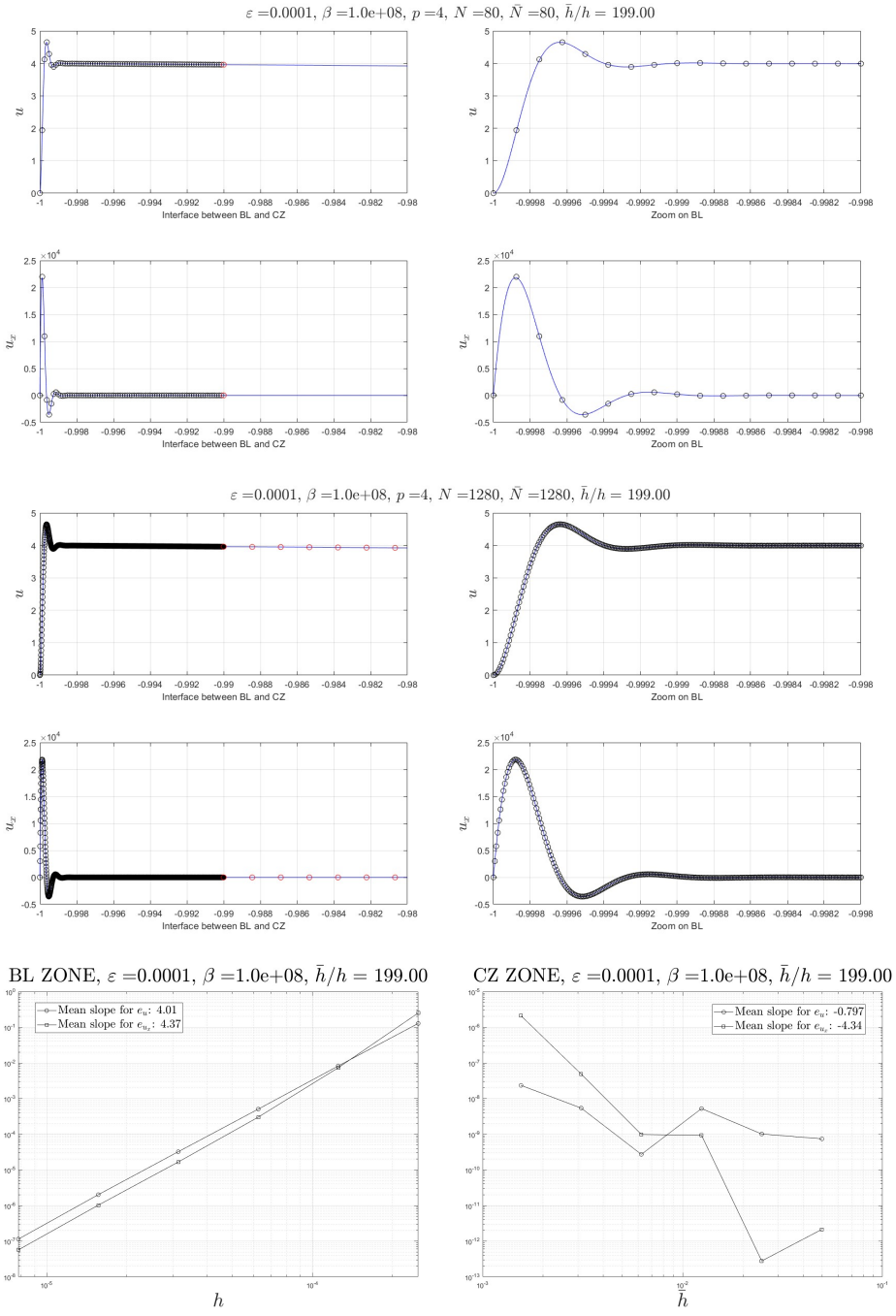

FIGURE 7. Munk-Stommel Equation (MK-1D) discretized with the scheme (3.15). Test case (2.8) with $p = 4$, $\varepsilon = 10^{-4}$, $\beta = 10^{8}$, $\gamma = 10^{-4}$. Coarse to fine grid ratio $\bar{h}/h = R \simeq 200$. Convergence is analyzed with grid sequence $(N, \bar{N})$ is $(40, 40), (80, 80), (160, 160), (320, 320), (640, 640), (1280, 1280)$.
The transmission node is located at $c = -0.99$. The convergence rate is around 4 in the BL zone for u and $\frac{d}{dx}u$. The computer accuracy is obtained in the CZ zone. The maximum relative error is close to 10^{-7} for u and u' in the BL zone.

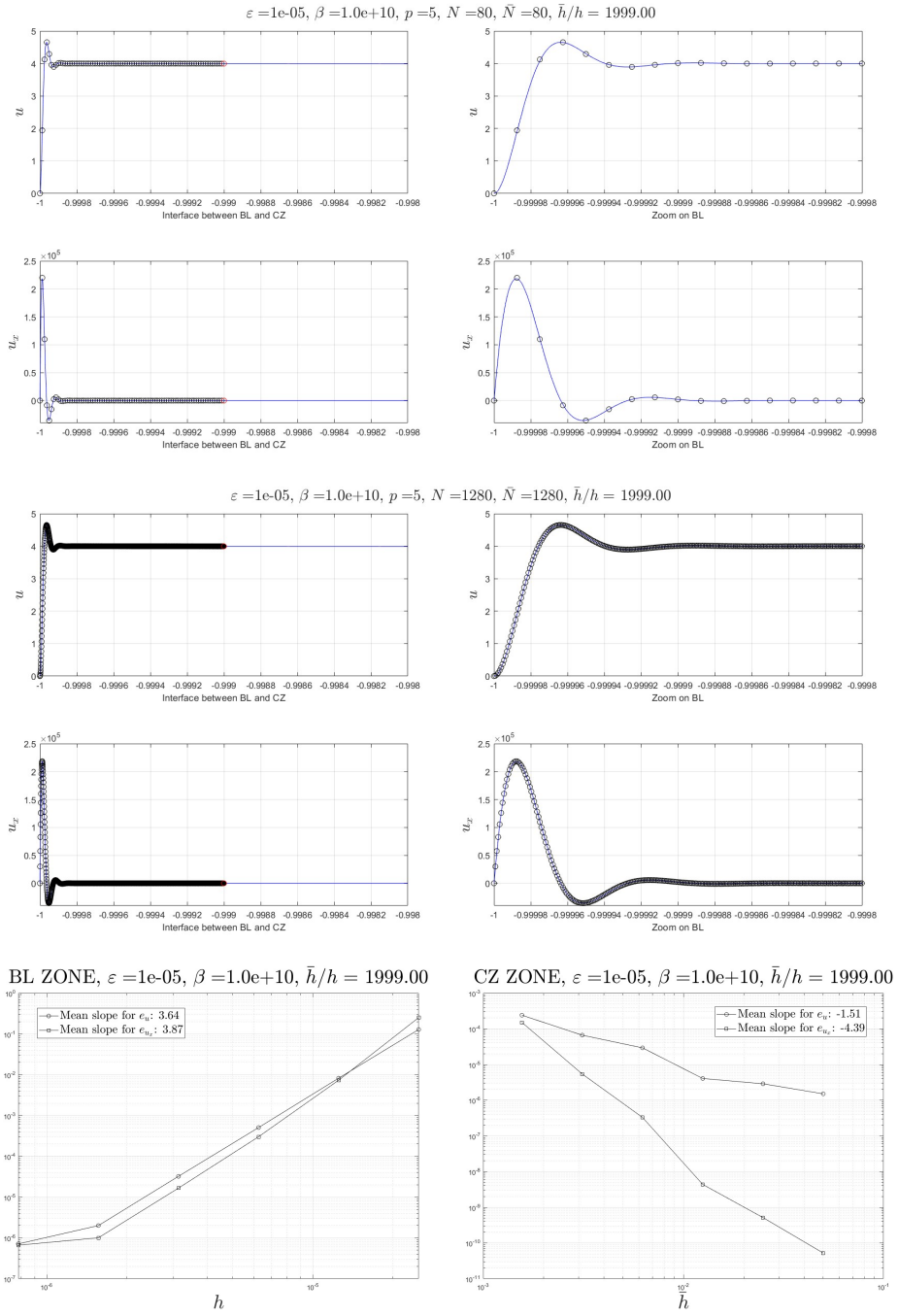

FIGURE 8. Munk-Stommel Equation (MK-1D) discretized with the scheme (3.15). Test case (2.8) with $p = 5$, $\varepsilon = 10^{-5}$, $\beta = 10^{10}$, $\gamma = 10^{-5}$. Coarse to fine grid ratio $\bar{h}/h = R \simeq 2000$. Convergence is analyzed with grid sequence $(N, \bar{N})$ is $(40, 40), (80, 80), (160, 160), (320, 320), (640, 640), (1280, 1280)$.
The transmission node is located at $c = -0.999$. The convergence rate is around 4 in the BL zone. The computer accuracy is obtained in the CZ zone. The maximum relative error is close to 10^{-6} for u and u' in the BL zone.